# GUARD RING INDUCED DISTORTION OF THE STEADY VELOCITY PROFILE IN A PARALLEL PLATE RHEOMETER

SVEN PIEPER<sup>1</sup> AND HANS-JOACHIM SCHMID<sup>1</sup>

<sup>1</sup>Paderborn University, Warburger Straße 100, 33098 Paderborn, Germany

\* Corresponding author: hans-joachim.schmid@upb.de

Received: 28.6.2016, Final version: 6.9.2016

#### **ABSTRACT:**

The shape and fracture of the free surface frequently limits the measuring range and impedes the use of optical velocimetric techniques in parallel plate and cone plate setups. To prevent this, various kinds of edge guards are often employed. In the present study, we elucidate how an edge guard distorts the steady velocity profile in a parallel plate setup. To this end, we analyzed the velocity field of a strongly shear-thinning fluid, a Newtonian fluid and a set of suspensions via particle image velocimetry in a parallel plate device. Several guard ring sizes were studied. The distortion is described by a simple three parameter model. These parameters are mostly constant for different fluids and suspensions with particle volume fractions below 45%. With increasing radius, the guard ring's influence approaches a limiting value that we attribute to the influence of the fluid surrounding the gap. Our results indicate a limiting ratio of the difference between plate radius and guard to gap size that should always be exceeded. In the presence of a guard ring, even Newtonian fluids do not exhibit a constant shear rate for most radial distances within the gap. This distortion of the velocity field challenges the simple superposition approach of unguarded device and guard influence that is prevalent in the literature.

#### **KEY WORDS:**

Parallel plate, guard ring, edge guard, suspension, edge fracture

#### 1 INTRODUCTION

The parallel plate (PP) and the cone plate (CP) setup are among the most frequently used devices in rheology. A major disadvantage of these systems is that the upper limit of the accessible shear rate range is not determined by the rheometer's specifications but by the onset of edge fracture. A factor that is mostly determined by the sample's properties and that frequently evokes inaccurate rheometric results. Even if no edge fracture occurs, the shape of the meniscus can affect the signal recorded by the instrument [1–4] and complicate optical accessibility [5], which is a prerequisite for techniques such as particle image velocimetry (PIV).

Several approaches to avoid these problems have been proposed. Gleissle [6] fitted a circumferential guard to a CP system to extent the measuring range for normal stresses to higher shear rates. This resulted in an actually steady torque signal for higher shear rates that he could not obtain without the guard ring. In a subsequent study, Mall-Gleissle et al. [7] shifted the shear stress obtained with the same setup to the values

that were obtained without the guard ring in a range that is accessible to both setups. Thus, they determined an offset factor that was used to correct their results for the ring's influence. Another approach is the cone portioned plate (CPP) device [8], where only the inner part of the plate rotates and the outer annulus is fixed to the rheometers frame. The guard ring is thus replaced with a stationary fluid and the free surface is removed from the sheared volume. Schweizer [9] compared the CPP setup to a conventional CP and found that the CPP geometry resulted in higher shear stresses and normal forces but concluded that these differences were negligible. Another study [10], specifically targeted at polymer solutions, came to a similar conclusion regarding the steady state.

To minimize optical distortion at the free surface, a common approach, used for example by Meeker et al. [11–12], is to wrap the edge with a transparent film. In their work, Meeker et al. only studied a single radial distance with a particle tracking technique. They reported that the film's influence was negligible for this position even though it resulted in an apparent shear stress rise

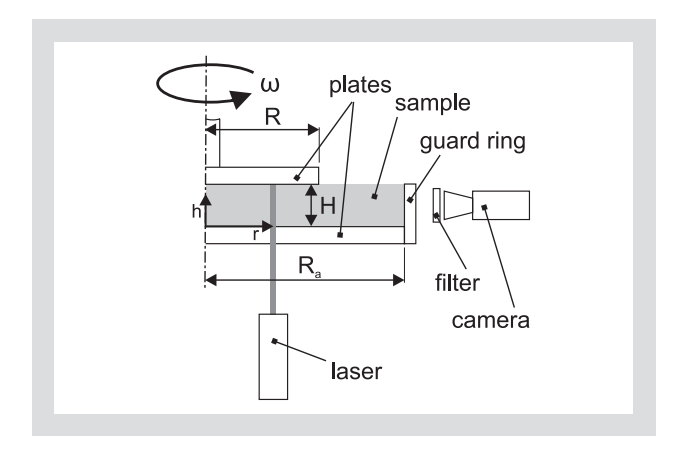


Figure 1: Schematic of the Rheo-PIV setup.

of approximately 20 %. Tapadia et al. [13] used such a film guard to study an entire CP device by optical velocimetric means and claimed that the film's influence was negligible. However, this was later challenged by Li et al. [14] who found that the results shown by Tapadia et al. were heavily influenced by edge effects and the film in particular. Furthermore, they concluded that the film significantly complicates the start-up flow behavior. Dimitriou et al. [15] showed that Rheo-PIV is possible without any edge guard if the meniscus does not deform much during the experiment. This is only possible for few fluid systems, since optical distortion at the free surface depends strongly on the sample's edge properties. The same group [5] also demonstrated that a planoconcave lens, placed extremely close to the rotating plate of a CP device is not suitable for fluids that do necessitate an edge guard as it adds too much local friction to the fluid in the setup.

Most of the studies discussed above simply assumed that the velocity profile in the gap remained unchanged and described the influence of the guard by superposition of torque contributions. However, with currently available PIV technology the actual velocity profile can be determined to improve on this approximation. In the present work, we focus on the PP setup as this is more important than CP in suspension rheology, which is the main topic of our group. We aimed to provide answers to the most essential questions that may be raised when an edge guard is applied. Mainly, whether the velocity profile in the gap remains intact as compared to the theoretical velocity in an unguarded PP device, how large the distance between the rotating plate and the guard should be to minimize distortion and whether the distortion depends solely on the geometry or on the sample's properties.

## 2 MATERIALS & METHODS

#### 2.1 SETUP

We used the parallel plate setup shown in Figure 1 that was mounted to an Anton Paar MCR501 stress controlled rheometer. Note that the radius of the rotating plate

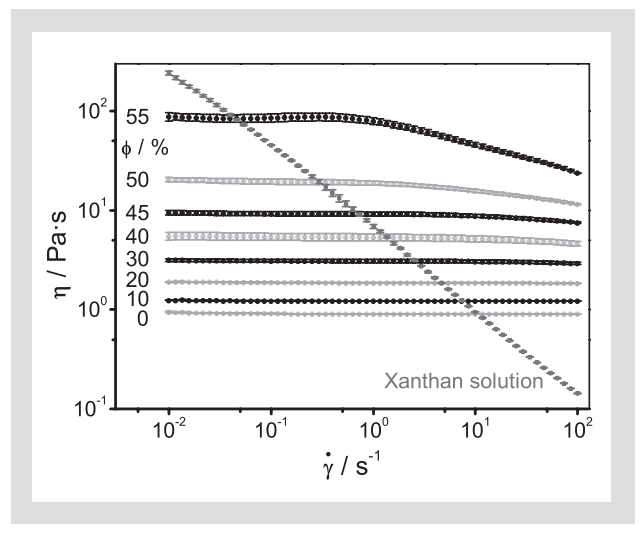
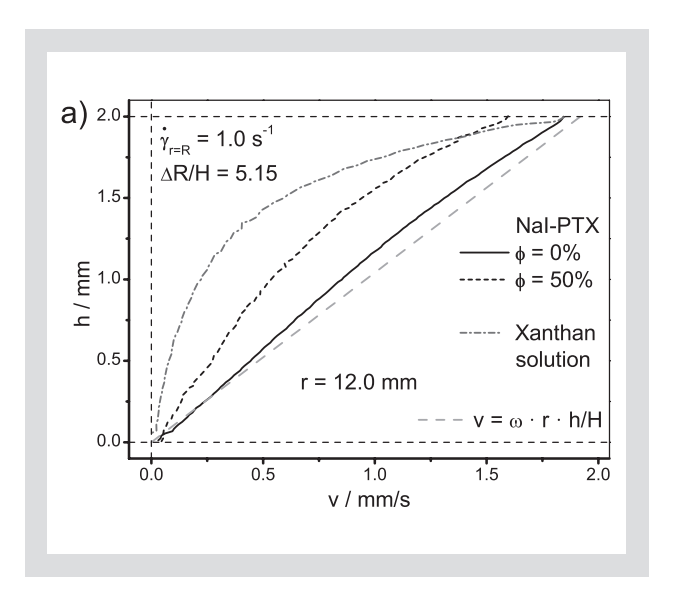


Figure 2: Viscosity plots of the NaI–PTX based suspensions and of the xanthan solution.

was R = 12.5 mm whereas various guard ring radii  $R_a$  were used. The ratio between radii difference and gap size  $(R_a - R)/H$  is denoted in the respective figures. The temperature was 20.5 ± 0.5 °C. The guard ring was planar to serve as a planoconcave lens as well as providing a smooth surface. Both the ring and the lower plate were made of PMMA, whereas the upper plate was covered with a smooth black surface that sufficiently inhibited reflection. A CCD camera DantecDynamics EO 4M recorded the light of fluorescent tracer particles (see 'Materials' section) in an illuminated plane that corresponded to a specified radial distance. The camera had a sensor resolution of 2048 times 2048 pixels. It was operated in single frame mode at acquisition frequencies between 1 and 15 Hz, depending on the flow velocity to be observed. We used a Blau Optoelektronik MVNano DL 520 nm 30 mW laser with included light sheet generating optics as light source. To ensure that only the fluoresced light was recorded, we placed a long pass edge filter, cut-off wavelength  $\lambda_c$  = 536.4 nm, in front of the camera. Because the light sheet was straight but the particle's trajectories curved, the visible particles in every image were distributed over a range of radial distances. From the width of the observation window, which was 2.00 mm, we estimated the maximum radial distance between two tracer particles in an image as 0.10 mm  $\langle \Delta r \langle$  0.18 mm. All other experimental parameters are denoted in the corresponding diagrams.

#### 2.2 IMAGE PROCESSING

First, all images were subjected to a low threshold high pass filter. This greatly reduced noise and computation time of the next step. The essence of standard PIV algorithms is the cross-correlation of defined interrogation areas of successive images. The correlation function maximum corresponds to the average displacement of the interrogation area in a time step, i.e. the inverse frame rate. The same method was used here. We adjusted the frame rate for every radial position and an-



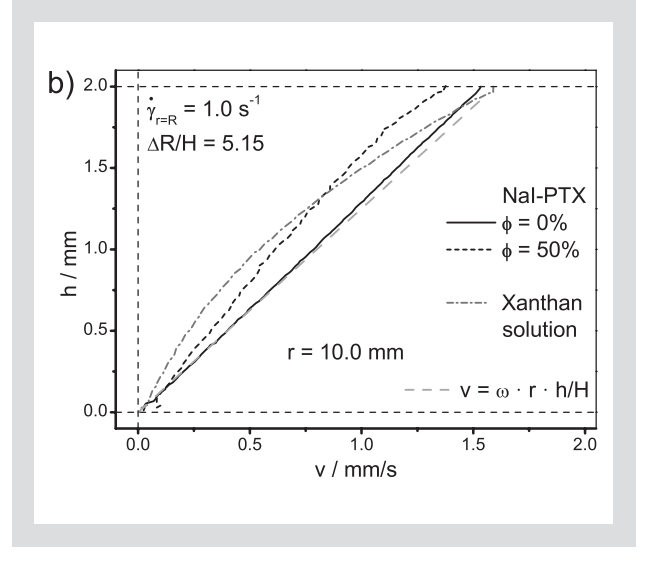


Figure 3: Circumferential velocity at (a) r = 12.0 mm and (b) r = 10.0 mm.

gular velocity to ensure that the maximum displacement between consecutive images did not exceed the maximum displacement detectible with the algorithm. The vertical size of the interrogation areas was 8 pixels. We estimated the vertical spatial resolution to be approximately equivalent to the tracer particle radius, i.e. 15  $\mu$ m, and slightly higher near the plates, as these cannot be penetrated by the particles. No noticeable flow was detected in the vertical direction and will therefore not be discussed below. Since the scope of the present study was steady shear flow, we averaged the velocity profile over 200 consecutive image pairs to obtain a 2D velocity field for every radial position and experimental parameter set.

A two-step process was employed to detect the plates. First, the average intensity distribution was calculated for every series of images. The gap was visible in the resulting average image as bright area. Standard edge detection algorithms were then used to detect the edges of the gap in this image. The gap size detected from the images and the nominal gap size agreed within 2%. However this does not account for deviations of the actual gap size such as errors during the determination of the zero gap position. The detection process was likely better than implied by the deviation percentage.

### 2.3 MATERIALS

We used CA30 poly(methyl methacrylate) (PMMA) spherical particles from Microbeads as tracers for the PIV measurements. These particles had a mean diameter of 30  $\mu$ m and a very narrow size distribution according to the supplier. The tracers were dyed with Rhodamine B by the following process: 0.75 g/l Rhodamine B were dissolved in ethanol at 60 °C. 20.0 g/l of particles were then added to the fluid and stirred for one hour at this temperature. After filtration, the particles were rinsed with pure ethanol. The concentration of these tracer particles was 0.20 % in all samples, which did not noticeably alter the rheological response. The suspen-

sion particles used in this work were PMMA spheres, trade name Degacryl M449, provided by Evonik Industries. The diameter range was 100 to 125  $\mu$ m obtained via air jet sieving. The refractive index of these particles was  $n_{D20}$  = 1.4900 and the density  $\rho$  = 1190 kg/m³ at the average laboratory temperature of 20.5 °C.

We chose the matrix fluid to closely match the particle's refractive index and density. Refractive index matching is a prerequisite for transparent suspensions that are mandatory for the application of PIV. The matching density was necessary to allow for sufficient degassing by sonication. A density mismatch may lead to both sedimentation and cause a yield stress [16] that further obstructs the degassing process. Furthermore, a fluid with a high ion content was chosen to prevent electrostatic interactions of the particles [17]. The Newtonian matrix fluid, a mixture of 54.76 wt% Triton-X100, 25.23 wt% poly(ethylene glycol) 400 and 20.01 wt% of a 60.00 wt% solution of sodium iodine in deionized water, exhibited a dynamic viscosity of  $\eta_o$  = 0.908 Pas. Since both refractive index and density are never perfectly uniform in a batch of particles,  $\Delta n_{D20} \approx 3.10^{-4}$  and  $\Delta \rho / \rho \approx 2.10^{-3}$ were found to be the limiting tolerances. This fluid is referred to as "NaI-PTX" in the remainder of the study.

A shear thinning fluid was prepared by dispersing 0.50 wt% xanthan gum in 25.0 wt% poly(ethylene glycol) 400 and then adding deionized water under vigorous stirring. This mixture was slightly opaque but transparent enough to allow for robust PIV measurements. Viscosity plots of all of the suspensions, the unfilled NaI-PTX fluid and of the xanthan solution are shown in Figure 2. These were recorded with a commercial concentric cylinder cell of the Searle type for the MCR501 Anton Paar rheometer mentioned in the "Setup" subsection. As these plots demonstrate, all of the suspensions exhibited fairly Newtonian behavior at shear rates below 1.0 s<sup>-1</sup> and only the highest concentrations were shear-thinning at higher shear rates. As intended, the xanthan solution was strongly shear-thinning in the entire measuring range.

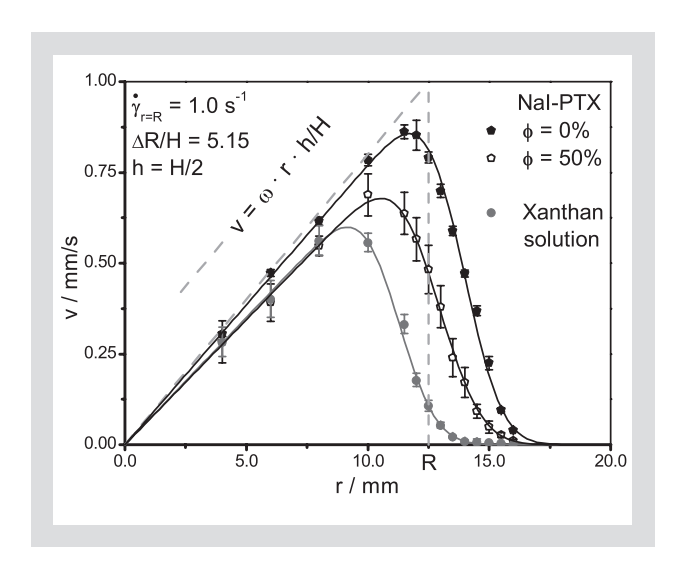


Figure 4: Circumferential velocity in the gap's vertical central plane (solid lines correspond to the model function).

#### 3 RESULTS & DISCUSSION

The circumferential velocity of two vertical sections is shown in Figure 3. These sections correspond to two radial positions in the gap close to the edge of the rotating plate. As these plots show, the slope of the Newtonian fluid's velocity profile was fairly close to the standard theory for parallel plate rheometers, even close to the edge. The dense suspension deviated from this slope and exhibited a noticeable curvature. This deviation decreased with increasing distance to the edge of the rotating plate, i.e. towards the axis of rotation (Figure 3b). The dense suspension also seemed to slip at the upper plate but not at the lower plate. Intense particle-particle interactions probably impeded the propagation of shear flow in the bulk and flow was partially localized to the thin depleted fluid layer that is characteristic of apparent slip. Due to the finite size of the tracer particles, measurement uncertainty was slightly larger near the plates. The slight slip of the Newtonian fluid in Figure 3 was probably a consequence of this effect.

The extremely shear-thinning fluid deviated much more at the vertical center but approached the expected values near the top plate. This resulted in a strong curvature of the profile with high local shear rates in the top half of the gap and shear rates that were lower than expected in the bottom half. These curves agree qualitatively with the study of Li et al. [14] for polymer solutions, which are also strongly shear-thinning. As for the suspension, the curvature of the shear-thinning fluid's profile was also less pronounced at the lower radial distance. A horizontal section in the vertical center of the velocity field is shown in Figure 4. As expected from the vertical sections, the Newtonian fluid agrees quite well with the standard PP theory over most of the moving plate's radius. However, the circumferential velocity starts to decrease in the gap and not just outside of it. Peak velocity occurs much earlier in a dense suspension and earlier still in the shear-thinning fluid.

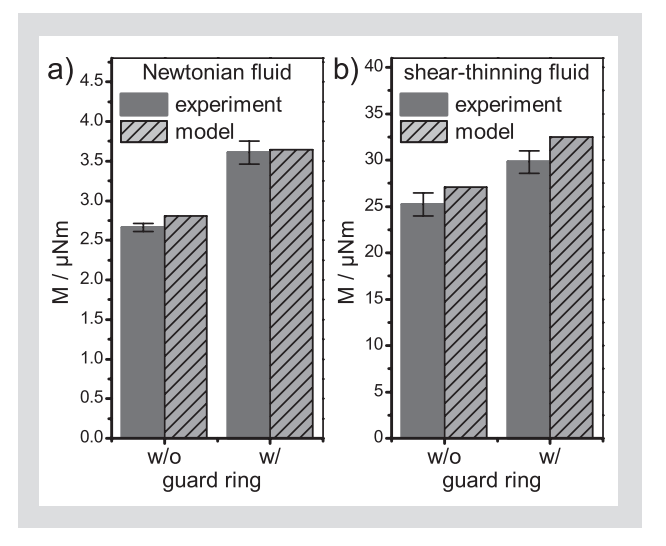


Figure 5: Torque predicted by the model compared to experimental values for a Newtonian fluid b shear–thinning fluid  $(\Delta R/H = 5.15, H = 2.0 \text{ mm}, \dot{\gamma} r = R = 1.0 \text{ s}-1).$ 

A simple model that describes the circumferential velocity v as a function of both the radial distance r and the vertical position h is given in Equation 1. This model equation can be applied to the entire radial distance range  $o \le r \le R_a$ .

$$v = \omega \frac{h}{H} r k_s (1 - F(r))$$
(1)

where F(r) is a cumulative normal distribution function with mean value  $\mu$  and standard deviation  $\sigma$  (Equation 2).

$$F(r) = \frac{1}{2} \left( 1 + erf\left(\frac{r - \mu}{\sigma \sqrt{2}}\right) \right)$$
 (2)

The slope parameter  $k_s$  accounts for the deviation of the angular velocity from the expected value, for example in the dense suspension due to slip at the upper plate, and should be between zero and one. The mean value  $\mu$  of the distribution function, referred to as position parameter here, corresponds to the inflection point of the velocity decay outside of the gap. The standard deviation  $\sigma$ , referred to as edge parameter, scales the rate of decay. For  $k_s$  = 1,  $\mu$  = R and  $\sigma$  = 0 the velocity profile is equivalent to the theoretical shape expected for standard parallel plate devices. Thus, we were able to evaluate the shape of a radial velocity profile and its deviation from standard theory by comparing these model parameters and their changes with regard to different experimental parameter sets. While this model worked reasonably well for two dimensional sections of the gap as shown in Figure 4, it certainly has its limitations. Even with three parameters, the model still assumes that the velocity is proportional to the vertical coordinate h. This may reasonably approximate the Newtonian fluid shown in Figure 3, as well as both the suspensions and the shear-thinning fluid some distance from the edge.

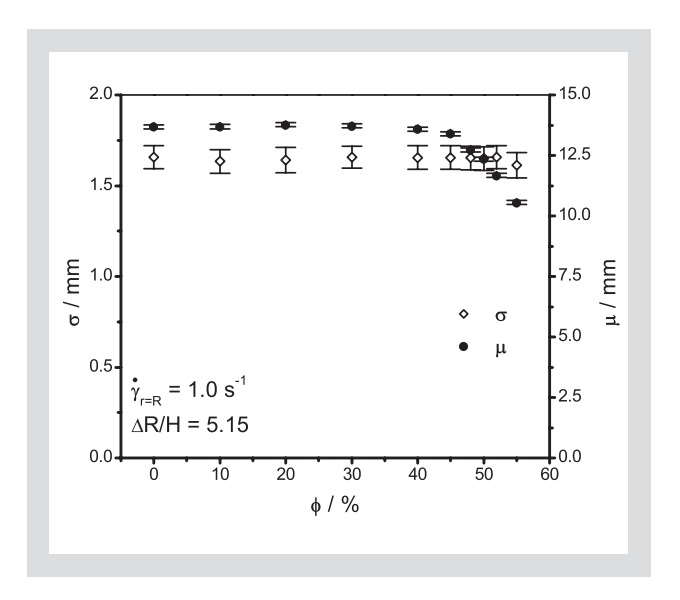


Figure 6: Edge and position parameter as a function of the particle volume fraction.

However, the information of the curved profile in Figure 3a is reduced to its average slope. A simple way to assess the quality of the model approximation is to compare the steady torque predicted by the model to the experimental results. The torque is especially suitable because it is an integral parameter, i.e. it accounts for the entire shear field, and it is experimentally accessible without relying on further assumptions. We calculated the steady torque M (Equation 3) for the Newtonian fluid, as best case, and the xanthan based shear thinning fluid, as worst case. This was performed for the setups with and without guard ring.

$$M = 2\pi \int_{o}^{R_a} \eta \dot{\gamma} r^2 dr \tag{3}$$

We used the viscosity from the plots shown in Figure 2 and determined the shear rate by applying the definition given in Equation 4 to the model Equation 1 and the standard PP velocity function respectively.

$$\dot{\gamma} = \frac{dv}{dh} \tag{4}$$

Experimental values of the torque without guard ring were obtained by applying standard edge trimming. Since the curvature of the Newtonian fluid's velocity plots (Figure 3) is low, model prediction and experimental values shown in Figure 5 agreed quite well. For the shear-thinning fluid, the predicted value exceeded the experimental result for both the guarded and the unguarded setup. The difference was only slightly larger than the measurement uncertainty of the experimental torque, but much greater than for the Newtonian fluid. It was also present for the setup without guard ring, indicating that edge effects already have a significant influence at the low shear rate chosen here. The

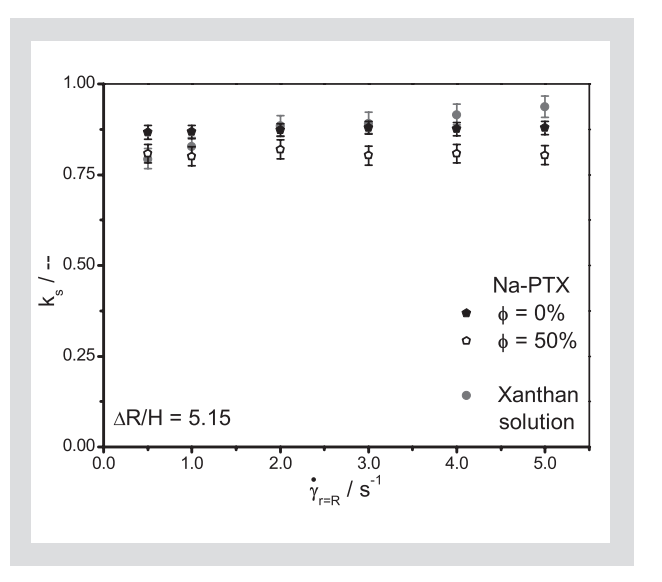
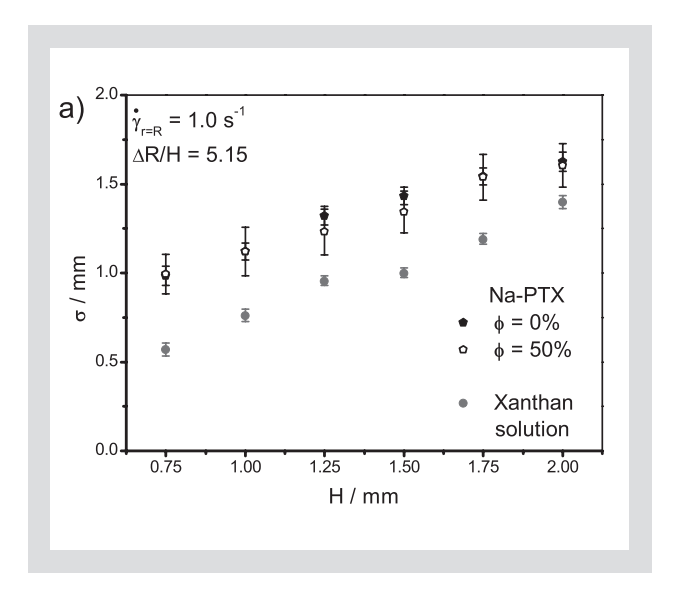


Figure 7: Slope parameter versus apparent shear rate.

difference between the experiment with and without guard was 35.5 % for the Newtonian fluid and 18.0 % for the shear thinning sample which agrees with the results of Meeker et al. [11] [12].

Nonetheless, the model still proved valuable to quantify and discuss the average distortion of the velocity field with regard to various experimental conditions.

Figure 6 shows two of the three model parameters for one experiment as a function of the particle volume fraction. Most properties of a suspension, such as the dynamic viscosity, are very sensitive to changes of the particle volume content. However, the shape of the velocityprofile and thus the model parameters are very robust regarding this parameter. They are only affected at the highest concentrations. While the suspensions were also shear-thinning in this concentration range, none of them showed noticeable non-Newtonian behavior for the apparent shear rate used here. The concentration limit, approximately 45%, roughly corresponds to the onset of strong structuring for these particles [18]. Hence, it was probably the increase of mechanical particle-particle interactions that shifted the edge influence further into the sheared gap as indicated by the decrease of the position parameter. This also resulted in a progressive propagation of slip, localized at the upper plate, from outer to inner radial positions as flow was increasingly restricted by the surrounding stationary particles. As this slip occurred at radial positons beyond the peak velocity, it was not reflected in changes of the slope parameter. The underlying shape of the peak changed only slightly since both the edge parameter and the slope parameter (not shown) were not affected significantly. Standard PP rheometer theory assumes that the shape of the circumferential velocity profile is not affected by the angular velocity. This mostly held true for the guarded PP setup as well. The model parameters were invariant to changes of the apparent shear rate except for the slope parameter of the shear-thinning fluid (Figure 7).



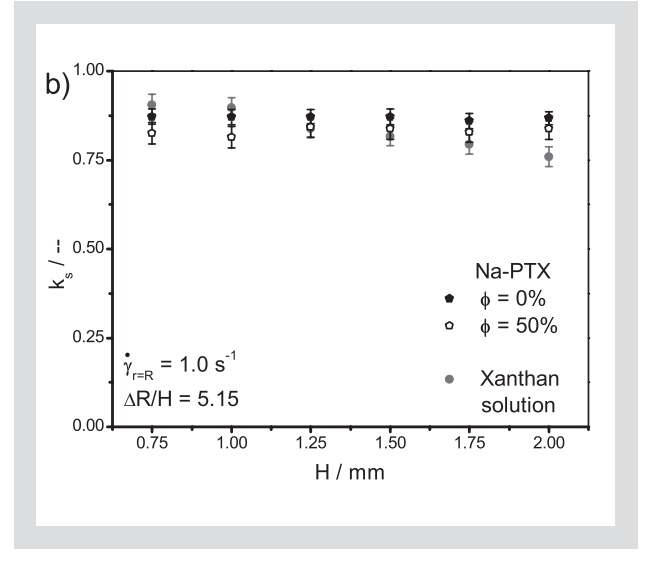


Figure 8: Model parameters as a function of the gap height for (a) edge and (b) slope parameter.

In contrast to the Newtonian fluid and the suspensions, the shear-thinning fluid's slope parameter actually approached  $k_s = 1$  for increasing apparent shear rates, i.e. angular velocities. Thus, the results of a guarded PP setup actually improved for shear thinning fluids if the apparent shear rate is increased. While the other parameters were not affected, a changing shape of the velocity profile also means that the results obtained with different shear rates cannot be compared without accounting for this effect. To understand this effect, it is more convenient to argue based on the shear stress, rather than shear rate. Because the torque is distributed over a larger surface area at the lower than at the upper plate, the shear stress is also a function of the vertical coordinate and reaches its maximum at the upper plate. Higher local shear stresses result in higher local shear rates. This effect is small for Newtonian fluids, as displayed in Figure 3a. But for shear thinning fluids, the absolute viscosity difference for a given shear stress difference is lower for higher shear stresses than for lower levels. Thus, the absolute shear rate difference along the vertical coordinate is also lower for higher shear stresses and the curvature of the velocity profile decreases. The slope parameter, which represents the average deviation from unguarded PP systems, therefore also decreases.

By far the most important parameter for guarded systems of any kind is the gap height. While the edge parameter was insensitive to changes of the angular velocity, it scaled linearly with the gap height as shown in Figure 8a. Users of a guarded setup are thus well advised to keep the gap small. The relationship between edge parameter and gap was linear, but they were not proportional, i.e. even if the gap approached zero the velocity field would not conform to the ideal shape. The other two model parameters were generally not affected by the gap size. The only exception in this regard was the slope parameter of the shear-thinning fluid (Figure 8b). It decreased slightly with increasing gap size. Thus reducing the gap size of a guarded setup would be bene-

ficial both regarding the velocity profile in the gap as well as its decay outside of it.

Supposedly, the main advantage of the CPP over other guarded systems is that it does not require an additional film or ring which is believed to affect the velocity field more than the additional fluid surrounding the sheared portion. In our own experiments, we found that the surrounding fluid created the majority of the distortion and the ring's influence was small. Figure 9 shows the edge parameter as a function of the relative radii difference  $\Delta R/H$ . This value increased if the distance between guard ring and rotating plate was larger. As is demonstrated by the graph, the shape of the velocity field outside of the gap was not affected by the ring for values of  $\Delta R/H > 3$ . Since the position parameter was generally lower for the shear-thinning fluid, it was still less influenced by the presence of the ring. Since the shape of the velocity field stabilizes for very small fluid reservoirs surrounding the sheared part, we conclude that it is entirely irrelevant if the surrounding fluid is contained by a film or tube.

#### 4 CONCLUSION

The distortion of the steady velocity field in a parallel plate device was shown to be effectively characterized by a simple three parameter modification of the standard theoretical velocity function. These model parameters were largely independent of geometric factors. The exception to this was the rate of velocity decline outside of the gap. This parameter scaled linearly with the gap height. As the parameters were independent of the guards radius for a ratio of  $\Delta R/H > 3$ , we conclude that this limiting ratio should always be exceeded when experiments are designed that necessitate an edge guard. Regarding the different fluids, not even the Newtonian fluid exhibited a constant shear rate for outer radial positions within the sheared gap. However, this behavior was independent of the fluid for all the

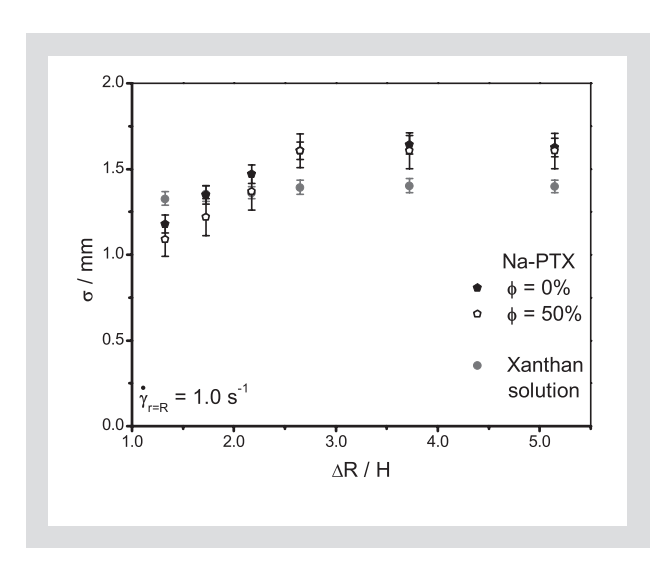


Figure 9: Edge parameter for varying ratio of radii difference to gap height.

homogeneous samples studied here and also for most of the suspensions. Only when the particle volume fraction approached 45% stronger distortions of the velocity field occurred. The shear thinning fluid exhibited the strongest distortion in both vertical and horizontal sections of the gap. It was also distorted by factors, such as shear rate, that did not affect the Newtonian fluid or the suspensions.

While the model used in the present work can also predict the steady torque quite accurately, this presupposes that the parameters are well known for the respective fluid. Furthermore, it does not eliminate the problem that, in the presence of a guard ring, a representative shear rate is difficult to define. Since even Newtonian fluids exhibited a distorted velocity field, the previously prevalent approach, i.e. the superposition of unguarded device and guard influence, should be avoided if possible. An edge guard can still be useful to extent the measuring range that would otherwise not be accessible, if the distortions are properly accounted for. While the model parameters were only marginally influenced by experimental factors for the Newtonian fluid and the suspensions, caution is advised when using shear thinning fluids as these are more strongly distorted and even comparing measurements under identical conditions is problematic. While it should be good practice for any type of measurement, it is especially important for guarded setups to note the exact experimental conditions and geometric dimensions to prevent inappropriate conclusions.

#### **ACKNOWLEDGEMENTS**

The PIV equipment was funded by Deutsche Forschungsgemeinschaft (DFG) under grant INST 214 84-1 FUGG. We are grateful for the Degacryl M449 particles that were provided by Evonik Industries.

#### REFERENCES

- [1] Griffiths DF, Walters K: On edge effects in rheometry, J. Fluid Mech. 42 (1970) 379–399.
- [2] Shipman RWG, Denn MM, Keunings R: Free-surface effects in torsional parallel-plate rheometry, Ind. Eng. Chem. Res. 30 (1991) 918–922.
- [3] Olagunju DO: Effect of free surface and inertia on viscoelastic parallel plate flow, J. Rheol. 38 (1994) 151–168.
- [4] Johnston MT, Ewoldt RH: Precision rheometry: Surface tension effects on low-torque measurements in rotational rheometers, J. Rheol. 57 (2013) 1515–1532.
- [5] Dimitriou CJ, Casanellas L, Ober TJ, McKinley GH: Rheo-PIV of a shear-banding wormlike micellar solution under large amplitude oscillatory shear, Rheol. Acta 51 (2012) 395-411.
- [6] Gleissle W: Druckverteilung im Spalt eines Kegel-Platte-Rheometers bei der Scherung viskoelastischer Flüssigkeiten mit hohen Schergeschwindigkeiten, Rheol. Acta 15 (1976) 305–316.
- [7] Mall-Gleissle SE, Gleissle W, McKinley GH, Buggisch H: The normal stress behaviour of suspensions with viscoelastic matrix fluids, Rheol. Acta 41 (2002) 61–76.
- [8] Meissner J, Garbella RW, Hosteller J: Measuring normal stress differences in polymer melt shear flow, J. Rheol. 33 (1989) 843–864.
- [9] Schweizer T: Comparing cone-partitioned plate and cone-standard plate shear rheometry of a polystyrene melt, J. Rheol. 47 (2003) 1071–1085.
- [10] Ravindranath S, Wang S-Q: Steady state measurements in stress plateau region of entangled polymer solutions:

  Controlled-rate and controlled-stress modes, J. Rheol. 52 (2008) 957–980.
- [11] Meeker SP, Bonnecaze RT, Cloitre M: Slip and flow in pastes of soft particles: Direct observation and rheology, J. Rheol. 48 (2004) 1295–1320.
- [12] Meeker SP, Bonnecaze RT, Cloitre M: Slip and flow in soft particle pastes, Phys. Rev. Lett. 92 (2004) 198302.
- [13] Tapadia P, Ravindranath S, Wang S-Q: Banding in entangled polymer fluids under oscillatory shearing, Phys. Rev. Lett. 96 (2006) 196001.
- [14] Li Y, Hu M, McKenna GB, Dimitriou CJ, McKinley GH, Mick RM, Venerus DC, Archer LA: Flow field visualization of entangled polybutadiene solutions under nonlinear viscoelastic flow conditions, J. Rheol. 57 (2013) 1411–1428.
- [15] Dimitriou CJ, McKinley GH, Venkatesan R: Rheo-PIV analysis of the yielding and flow of model waxy crude oils, Energy Fuels 25 (2011) 3040–3052.
- [16] Fall A, Bertrand F, Ovarlez G, Bonn D: <u>Yield stress and shear banding in granular suspensions</u>, Phys. Rev. Lett. 103 (2009) 178301.
- [17] Brown E, Forman NA, Orellana CS, Zhang H, Maynor B:

  Generality of shear thickening in dense suspensions,
  Nat. Mater. 9 (2010) 220–224.
- [18] Pieper S, Schmid H-J: Layer-formation of non-colloidal suspensions in a parallel plate rheometer under steady shear, J. Non-Newtonian Fluid Mech. 234 (2016) 1–7.

